1 **Distribution, chemical and molecular composition of high and**

2 **low-molecular-weight humic-like substances in ambient aerosols**

3 Xingjun Fan[a,b,*], Ao Cheng[a], Xufang Yu[a], Tao Cao[b,c], Dan Chen[a], Wenchao Ji[a],

4 Yongbing Cai[a], Fande Meng[a], Jianzhong Song[b,**], Ping'an Peng[b]

6 [a] College of Resource and Environment, Anhui Science and Technology University,

7 Fengyang 233100, P. R. China

8 [b] State Key Laboratory of Organic Geochemistry, Guangzhou Institute of

9 Geochemistry, Chinese Academy of Sciences, Guangzhou 510640, P. R. China

10 [c] University of Chinese Academy of Sciences, Beijing, 100049, PR China

12 * Corresponding authors

13 E-mail addresses: fanxj@ahstu.edu.cn (Xingjun Fan), songjzh@gig.ac.cn (Jianzhong

14 Song)

Abstract

Humic-like Substances (HULIS) encompass a continuum of molecular weight (MW) ranges, yet our understanding of how HULIS characteristics vary with MW is still limited and not well-established. In this study, a combination of ultrafiltration and solid-phase extraction protocols was employed to fractionate the high MW (HMW, >1 kDa) and low MW (LMW, < 1kDa) HULIS fractions from ambient aerosols collected during summer and winter at a rural site. Subsequently, comprehensive characterization by using total organic carbon, high-performance size exclusion chromatography (HPSEC), UV-vis and fluorescence spectroscopy, Fourier-transform infrared spectroscopy (FTIR), negative electrospray ionization high resolution mass spectrometry (ESI- HRMS) were conducted. The results revealed that HMW HULIS were dominated by larger-sized chromophores, substantially constituting a higher fraction of total organic carbon and UV absorption at 254 nm than LMW HULIS. While both HMW and LMW HULIS shared similar fluorophore types and functional groups, the former exhibited higher levels of humification and a greater presence of polar functional groups (e.g., -COOH, >C=O). HRMS analysis further unveiled that molecular formulas within HMW HULIS generally featured smaller sizes but higher degrees of unsaturation and aromaticity compared to those within LMW HULIS fractions. This observation suggests the possibility of small molecules assembling to form the HMW HULIS through intermolecular weak forces. Moreover, HMW HULIS contained a higher proportion of CHON but fewer CHO compounds than LMW HULIS. In both HMW and LMW HULIS, the unique molecular formulas were

39 primarily characterized by lignin-like species, yet the former displayed a prevalence

40 of N-enriched and highly aromatic species. Additionally, HMW HULIS contained

41 more unique lipids-like compounds, while LMW HULIS exhibited a distinct presence

42 of tannin-like compounds. These findings provide valuable insights into the

43 distribution, optical properties, and molecular-level characteristics of HULIS in

44 atmospheric aerosols, thereby advancing our understanding of their sources,

45 composition, and environmental implications.

46

47 **Keywords:** Humic-Like Substances, molecular weight fractionation, optical

48 properties, high-performance size exclusion chromatography, negative electrospray

49 ionization-high resolution mass spectrometry

50

1. Introduction

HUmic-Like Substances (HULIS) are complex and heterogeneous mixtures of water-soluble organic matters (WSOM) that are of great importance in the atmospheric environment. They usually share similar physicochemical properties (e.g., acidity, absorption, fluorescence, functional groups) with naturally occurring humic substances (Graber and Rudich, 2006; Zheng et al., 2013) and are prevalent in fog, clouds, rainwater and ambient aerosols (Birdwell and Valsaraj, 2010; Fan et al., 2016a; Santos et al., 2012). With substantial hygroscopic and surface-active properties, HULIS enhance the hygroscopic growth of particles, thereby contributing to the formation of the cloud condensation nuclei and ice nuclei (Chen et al., 2021a; Dinar et al., 2007). Moreover, acting as an important component of brown carbon (BrC), HULIS effectively absorb near-ultraviolet and visible light, thus influencing the global radiative balance and atmospheric chemistry processes (Bao et al., 2022; Zhang et al., 2020). Furthermore, HULIS have the potential to catalyze the formation of reactive oxygen species, leading to potential adverse health effects (Ma et al., 2019; Zhang et al., 2022b).

The chemical composition of atmospheric HULIS exhibit significant heterogeneity and typically comprises macromolecular compounds containing aromatic rings with highly conjugated structures, as well as long-chain hydrocarbon with polar groups (e.g., -OH, -COOH, -NO$_2$) (Fan et al., 2013; Huo et al., 2021). To unravel the structural characteristics and properties of HULIS, a range of analytical techniques, including absorption and fluorescence spectroscopy, Fourier transform

73   infrared spectroscopy (FTIR), nuclear magnetic resonance spectroscopy (^{1}H NMR),

74   have been utilized (Huo et al., 2021; Qin et al., 2022; Zou et al., 2020). These studies

75   have provided insights into the overall structural characteristics of complex HULIS,

76   including their abundances, chemical and optical characteristics (Huo et al., 2021;

77   Mukherjee et al., 2020; Win et al., 2018; Zhang et al., 2022b; Zheng et al., 2013). In

78   recent years, high-resolution mass spectrometry (HRMS) techniques, such as Fourier

79   transform ion cyclotron resonance mass spectrometry (FT-ICR-MS) and orbitrap

80   HRMS, in combination with electrospray ionization (ESI), have emerged as powerful

81   tools for elucidating the molecular-level characteristics of HULIS (Lin et al., 2012;

82   Sun et al., 2021; Wang et al., 2019; Zou et al., 2023). By utilizing HRMS, researchers

83   have gained deeper insights into the complexity and chemical heterogeneity of

84   HULIS at the molecular level.

85   Operationally, HULIS are defined as the hydrophobic fraction of water-soluble

86   organic matter (WSOM) typically extracted through solid-phase extraction (SPE)

87   protocol (Fan et al., 2012; Zou et al., 2020). Thus, the abundance and characteristics

88   of HULIS are contingent upon the chemical composition of WSOM. Previous studies

89   have shown that aerosol WSOM, often seen as water-soluble brown carbon (BrC), are

90   comprised of a continuum of molecular weight (MW) species, as revealed by

91   high-performance exclusion chromatography (HPSEC) analysis (Di Lorenzo et al.,

92   2017; Fan et al., 2023; Wong et al., 2019). These studies have highlighted that BrC

93   typically consist of both high-MW (HMW) and low-MW (LMW) chromophores in

94   various aerosols. For example, BrC emitted from fresh biomass burning (BB) are

95   dominated by low MW chromophores (Di Lorenzo et al., 2017; Wong et al., 2019).

96   However, BrC derived from aged BB aerosols and ambient aerosols tend to possess

97   more HMW chromophores that are highly chemically resistant (Di Lorenzo et al.,

98   2017; Fan et al., 2023; Wong et al., 2019). Further characterizations of different MW

99   BrC can be conducted using an ultrafiltration (UF) protocol (Fan et al., 2021). This

100   approach enabled researchers to obtain the distributions of content, chromophores and

101   fluorophores within various MW BrC fractions. Despite these advancements, the

102   chemical structures and molecular composition of different MW HULIS fractions

103   remain poorly understood. Consequently, a combination of UF and SPE protocols for

104   the fractionation and characterization of MW-separated HULIS is crucial, as it not

105   only provides insights into MW distributions but also illuminates the chemical

106   heterogeneities of aerosols HULIS.

107   In this study, a combination of UF-SPE isolation protocol was developed to

108   fractionate and characterize the MW HULIS fractions. Two distinct sets of ambient

109    $PM_{2.5}$ samples collected during summer and winter periods were utilized to facilitate a

110   comparative analysis of MW HULIS. Initially, the WSOM were fractionated into

111   high-MW (HMW, >1 kDa) and low-MW (LMW, <1 kDa) species using the UF

112   protocol. Subsequently, the resulting MW WSOM fractions underwent SPE to obtain

113   different MW HULIS fractions. The obtained HMW and LMW HULIS fractions were

114   comprehensively characterized using advanced analytical techniques, including total

115   organic carbon analysis, UV-vis and fluorescence spectroscopy, HPSEC, and HRMS

116   to unveil their abundances, absorption and fluorescence properties, and molecular

characteristics. The findings of this study hold great significance in advancing our understanding of the definition and molecular profiles of HULIS, as well as facilitating further investigations into their potential impacts on the atmospheric environment.

2. Materials and methods

2.1. Atmospheric fine particles sampling

Atmospheric $PM_{2.5}$ were sampled on the rooftop of a building within the campus of Anhui Science and Technology University (32.21ºN, 118.72ºE), around 20 m above ground level. Detailed information regarding the sampling site can be found in our previous studies (Cao et al., 2022; Fan et al., 2021). The $PM_{2.5}$ samples were collected using a high-volume $PM_{2.5}$ sampler (JCH-1000, Juchuang Ltd., Qingdao) onto prebaked quartz fiber filters (8 × 10 inches, Whatman). Sampling took place from July 25 to August 12, 2021, during summer, and from December 19, 2021 to January 6, 2022, during winter. Blank filters were also collected as control samples. All aerosol $PM_{2.5}$ filter samples were stored at -20 ºC in a freezer prior to analysis. The atmospheric pollutant data (NO_2, SO_2 and O_3) near sampling site during sampling period were obtained from the website (https://www.aqistudy.cn) and are summarized in Table S1. Additionally, the fire spots were investigated using data from the website (https://firms.modaps.eosdis.nasa.gov/map/) and are visualized in Fig. S1.

2.2. Application of UF-SPE for isolating MW HULIS fractions

139   Punches of summer and winter aerosol $PM_{2.5}$ filter samples were taken and

140   combined for the extraction of water-soluble organic matter (WSOM), respectively.

141   The filters were immersed in 300 mL of ultrapure water and subjected to

142   ultrasonication for 30 min. The resulting suspensions were then filtered through a 0.22

143   μm membrane (Φ 47 mm, Jinteng, China) to obtain bulk WSOM samples. These bulk

144   filtrates were further subjected to UF and SPE in tandem to obtain different MW

145   HULIS fractions. Please refer to Fig. S2 for a schematic representation of the

146   fractionation steps.

147   Before UF, the bulk WSOM were diluted to DOC concentration below 30 mg/L

148   to minimize the concentration effects and prevent the accumulation of organic matters

149   at the membrane surface during UF. The detailed UF procedure followed the profile

150   described in our previous study (Fan et al., 2021). Briefly, each bulk WSOM solution

151   was passed through a pre-cleaned 1 kDa cut-off membrane in a stirred UF cell

152   (Amicon 8200, Millipore, USA), with a pressure at 0.2 MPa applied by ultrapure N_2.

153   The concentration factor was ~10. The resulting retentate was considered as HMW

154   (>1 kDa) WSOM, while the permeate solutions represented the LMW (<1 kDa)

155   WSOM. Finally, each MW fraction was diluted to the initial volume for further

156   treatment and analysis. Mass balances of WSOM during one-step UF process

157   generally ranged from 92% to 99%, as determined by total organic carbon (TOC) and

158   UV absorption at 254 nm (UV_{254}), indicating good performance of UF without

159   substantial loss or organic contamination.

160   Subsequently, SPE was applied to isolate the so-called HULIS fractions from the

bulk and each MW fraction of WSOM, following the protocol proposed in our previous studies (Fan et al., 2013; Zou et al., 2020). Briefly, the acidified aqueous samples were passed through pre-activated HLB columns (Waters Oasis, 500 mg/6 mL, USA). The fractions retained on the resins (referred to as HULIS) were eluted with pure methanol and dried using a gentle stream of pure N_2. Finally, the bulk, HMW and LMW HULIS fractions were obtained. A blank filter control was performed using the same procedure described above, and the analysis signals of samples were corrected by blank control.

2.3. HPSEC analysis

The apparent MW distributions of MW HULIS fractions were analyzed using a high-performance liquid chromatography (HPLC) system (LC-20AT, Shimadzu, Japan) equipped with a refractive index detector (RID-10A, Shimadzu) and a diode array detector (SPD-M20A, Shimadzu). The wavelength of the diode array detector was set at 254 nm. Separation was performed using an aqueous gel filtration column (Polysep-GFC-P 3000, Phenomenex) preceded by a guard column (Polysep-GFC-P, Phenomenex). The mobile phase consisted of a mixture of water and methanol (90:10 v/v) containing 25 mM ammonium acetate (Di Lorenzo et al., 2017; Wong et al., 2019). The sample injection volume was 100 μL, and the flow rate was maintained at 1 mL min^{-1}. The HPSEC calibration was performed using a series of polyethylene glycol (PEG) standards (Kawasaki et al., 2011; Zhang et al., 2022c). The chromatographic peak areas were integrated to represent the abundances of

183 corresponding MW species. It should be noted that the MW values estimated here are

184 nominal rather than absolute due to the lack of appropriate standards for column

185 calibration (Fan et al., 2023; Wong et al., 2017).

186   The weight-average MW (Mw), number-average MW (Mn) and polydispersivity

187 (ρ), were determined using the following equations (Song et al., 2010):

$$Mw = \frac{\sum_{i=1}^{n} (h_i MW_i)}{\sum_{i=1}^{n} h_i} \tag{1}$$

$$Mn = \frac{\sum_{i=1}^{n} h_i}{\sum_{i=1}^{n} (h_i/MW_i)} \tag{2}$$

$$\rho = \frac{Mw}{Mn} \tag{3}$$

188 where h_i and MW_i are the absorption intensity of the chromatogram and the MW of

189 molecules corresponding to the ith retention time, respectively.

190

191 2.4. Measurements of WSOC content and optical properties

192   The concentration of water-soluble organic carbon (WSOC) in HMW and LMW

193 HULIS was measured using a Shimadzu TOC analyzer (TOC-VCPN, Japan)

194 following the non-purgeable organic carbon protocol.

195   The UV-vis spectra were recorded using a UV-vis spectrophotometer (UV 2600,

196 Shimadzu, Japan) over a wavelength range of 200-700 nm with 1 nm increments.

197 Excitation-emission matrix (EEM) spectra were determined using a fluorescence

198 spectrophotometer (F4600, Hitachi, Japan). The scanning ranges for excitation (Ex)

199 and emission (Em) wavelengths were 200-400 and 290-520 nm, respectively, with a

200 scanning speed was 12,000 nm/min.

201   To characterize the chemical and optical properties of MW HULIS fractions,

several commonly used spectra parameters were calculated, including the specific UV

absorbance at 254 nm ($SUVA_{254}$), the UV absorbance ratio between 250 and 365 nm

(E_2/E_3), spectra slope ratios (S_R), the absorption Angstrom exponent (AAE), and mass

absorption efficiency (MAE_{365}), fluorescence indices (FI), biological index (BIX), and

humification degree (HIX) (Fan et al., 2021; Li et al., 2022; Wu et al., 2021). Further

details can be found in Text S1 of the Supporting Information (SI).

2.5. HRMS analysis and data processing

The MW HULIS fractions were analyzed using a Q-Exactive mass spectrometer

(Thermo Scientific, Germany) equipped with a heated electrospray ionization (ESI)

source. The system operated in negative ESI mode with a resolution of 140,000 at m/z

= 200. The detection mass range was set from 60 to 900 m/z. To ensure accurate mass

measurements, mass calibration was carried out using a commercial standard mixture

of ESI-L Low Concentration Tuning Mix (G1969-85000, Agilent, USA). It's

important to note that the negative ESI source is more sensitive to detecting polar acid

compounds, and the reported specific chemical composition here represents a fraction

that is biasedly ionized in the negative ESI source, not the entire HULIS composition

(He et al., 2023; Song et al., 2022).

The acquired mass spectra were processed using Xcalibur software (V2.2,

Thermo Scientific). The mathematically possible formulas for all ions were calculated

with a signal-to-noise ratio (s/n) ≥ 5 using a mass tolerance of 5 ppm. The assigned

molecular formulas followed specific constraints, with limitations on the following

224 elements: C ≤ 50, H ≤ 100, O ≤ 20, N ≤ 3, S ≤ 2. Additionally, the elemental ratios of

225 H/C, O/C, N/ C, and S/C were constrained to the ranges of 0.3–3.0, 0–3.0, 0–0.5, and

226 0–2.0, respectively. The double-bond equivalents (DBE) and modified aromaticity

227 index (AI_{mod}) values of the assigned neutral assigned formula ($C_cH_hO_oN_nS_s$) were

228 calculated using the equations (4-5) (He et al., 2023; Song et al., 2022):

$$DBE = 1 + \frac{1}{2}(2c - h + n) \qquad (4)$$

$$AI_{mod} = \frac{1 + c - 0.5o - 0.5n - 0.5h}{c - 0.5o - n} \qquad (5)$$

229   The intensity-weighted molecular parameters (X_w) of MW, H/C, O/C, DBE, and

230 AI values were calculated according to the equation (6) (He et al., 2023; Zhang et al.,

231 2021; Zou et al., 2023):

$$X_W = \frac{\sum(I_i \cdot X_i)}{\sum I_i} \qquad (6)$$

232 where X represents the aforementioned parameters, and I_i denote the intensity for each

233 assigned formula i.

234

235 **3. Results and discussion**

236 3.1. Size and distribution of MW HULIS fractions

237 3.1.1. Molecular size of HMW and LMW HULIS

238   Due to the potential differences in molecular densities between the calibration

239 standards (PEG) and BB WSOC, the reported molecular weight of HULIS calculated

240 by HPSEC herein is only estimate. Fig. 1 shows the HPSEC chromatograms of MW

241 HULIS. Both HMW and LMW HULIS exhibit MW continuum distributions ranging

242 from 100 to 20,000 Da, which is consistent with the reported distributions of BrC in

243 BB-derived and various ambient aerosol in previous studies (Di Lorenzo et al., 2017;

244 Fan et al., 2023; Wong et al., 2017). However, the chromatographic patterns for HMW

245 HULIS clearly differ from those observed for LMW HULIS in both aerosol samples.

246 As seen in Fig. 1, HMW HULIS display an additional and stronger absorption peak at

247 around 4000 Da (peak *iii*), along with a more pronounced peak at 2200 Da (peak *ii*)

248 and a similar magnitude peak at 570 Da (peak *i*) compared to LMW HULIS. This

249 suggests that HMW HULIS contain the majority of larger molecular size

250 chromophores within the bulk WSOM. In addition, the magnitude peak at 570 Da

251 (peak i) in HMW HULIS may indicate the incorporation of small molecule through

252 weak interactions based on π–π and/or van der Waals forces between the HULIS

253 components (Fan et al., 2021; Piccolo, 2002).
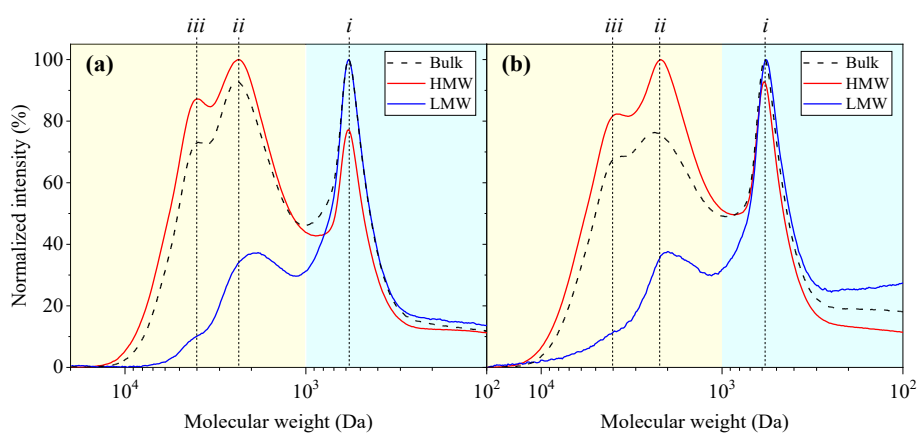
254

255 **Fig. 1.** Average HPSEC chromatograms of bulk, HMW and LMW HULIS fractions in

256 (a) summer and (b) winter aerosol, respectively. The yellow and cyan shadows

257 represent MW size regions of >1 kDa and <1 kDa, respectively.

258

259 Moreover, the molecular size of MW HULIS can be further reflected by the

260 differences in Mw and Mn. As listed in Table 1, the average Mw and Mn of HMW

HULIS are 2233-2315 and 654-707 Da, respectively, greatly larger than that of LMW

HULIS (989-1071 and 293-394 Da, respectively). Note that these values are estimates

rather than absolute, given the absence of the appropriate aerosol HULIS standards

(Fan et al., 2023; Wong et al., 2017). Moreover, these differences indicate that the

sources and formation processes of HMW HULIS may differ from LMW HULIS.

Many previous studies have demonstrated that fresh BB HULIS generally consist of

small molecular-sized chromophores (Di Lorenzo et al., 2018; Di Lorenzo et al., 2017;

Wong et al., 2017; Wong et al., 2019). However, a notable enhancement in the

formation of large molecular-sized chromophores has been found when they undergo

intricate atmospheric processes (Di Lorenzo et al., 2018; Di Lorenzo et al., 2017;

Wong et al., 2017; Wong et al., 2019). Based on these limited studies, it is suggested

that HMW HULIS, characterized by higher proportions of large-size chromophores

and the resulting larger apparent molecular size, might be associated with the products

from atmospheric aging process rather than being emitted directly by primary sources.

Table 1. The summary of typical quantity and quality parameters of each MW HULIS
fraction from BB and ambient aerosols.

		Summer			Winter		
		Bulk	HMW	LMW	Bulk	HMW	LMW
HPSEC-derived parameters	M_w	1975±13	2315±38	1071±24	1918±56	2233±42	989±67
	M_n	591±53	707±48	394±13	525±57	654±17	293±32
	ρ	3.4±0.3	3.3±0.2	2.7±0.2	3.7±0.3	3.4±0.2	3.4±0.2
HULIS/WSOM (%)[a]	TOC	65±1	68±1	51±2	63±2	67±2	41±1
	UV_{254}	66±5	65±2	55±4	67±1	65±1	61±2
Optical parameters	E_2/E_3	12.02±0.54	11.72±0.31	14.98±0.98	6.30±0.24	6.54±0.16	7.24±0.43
	MAE_{365}	0.21±0.02	0.23±0.01	0.20±0.01	1.04±0.02	1.06±0.01	0.88±0.00

	AAE	7.11±0.32	7.59±0.00	8.25±0.23	6.66±0.06	6.25±0.06	7.28±0.03
	FI	2.00±0.04	1.99±0.03	2.04±0.05	2.06±0.01	1.97±0.03	2.25±0.02
	BIX	0.95±0.01	0.86±0.07	1.02±0.01	0.96±0.01	0.81±0.01	1.07±0.02
	HIX	2.42±0.06	2.43±0.04	2.40±0.05	3.13±0.25	5.64±0.34	1.94±0.16

[a] The ratios of contents of SPE-isolated HULIS fractions to that of corresponding WSOM fractions determined by TOC and/or absorbance at 254 nm (UV_{254}).

3.1.2. Relative abundances of HMW and LMW HULIS

The contribution of MW-HULIS fractions to their corresponding MW-WSOM fractions, quantified in terms of TOC and UV absorption at 254 nm for both summer and winter aerosols are summarized in Table 1. In general, the ratios of HULIS/WSOM of HMW fractions (in terms of TOC and UV254) (65-68%) were higher than the ratios (41-61%) observed for LMW fractions. This finding suggests that the higher presence of hydrophobic and conjugated aromatic structures in HMW WSOM, but more hydrophilic OC and non-aromatic species (e.g., aliphatic dicarboxylic acid) in the LMW WSOM (Fan et al., 2012; Zou et al., 2020).

Fig. 2 illustrates the distribution of distinct MW fractions within reconstructed WSOM, wherein "non-HULIS" refers to the content differences between the MW WSOM and its HULIS fractions. The HMW HULIS fraction contributed 39-41% of TOC and 40-47% of UV254 to the bulk WSOM. In contrast, the LWM HULIS fraction only make up a smaller proportion, accounting for 16-20% of TOC and 17-21% of UV254 within the bulk WSOM. Specifically, the ratios between HMW HULIS and LMW HULIS (H/L) ranged from 1.88 to 2.75 for both summer and winter aerosols in terms of either TOC or UV254. These findings emphasize that HMW HULIS

significantly dominate the bulk aerosol HULIS fractions. Notably, the H/L ratio for winter aerosols was higher than that for summer aerosols, suggesting that larger-sized HULIS contributed more to the bulk HULIS fractions in winter aerosols.
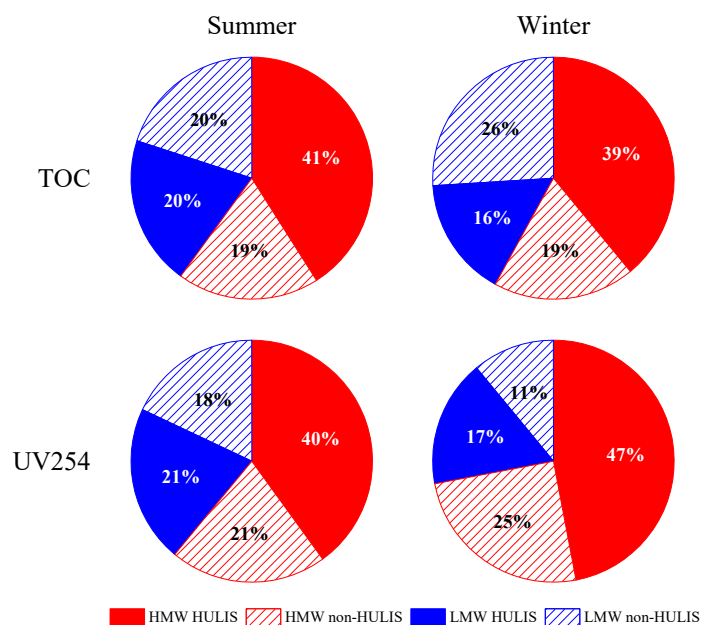
Fig. 2. Relative proportions of different MW fractions in summer and winter aerosols determined by TOC and UV254.

The non-HULIS fractions are also important constituents within aerosol WSOM, but exhibit some differences between HMW and LMW fractions. The contributions of HMW non-HULIS to bulk WSOM were ~19% as determined by TOC and 21-25% measured by UV254. In case of LMW non-HULIS, the contributions were higher in terms of TOC (20-26%) but lower in terms of UV254 (11-18%). These results indicate that the LMW WSOM contain a larger proportion of hydrophilic organic species with weaker light absorption.

3.2. Optical characteristics of MW HULIS fractions

314 3.2.1. Light absorption characteristics

315   The absorption spectra of MW HULIS fractions in ambient aerosols are shown in

316 Fig. S3. These spectra exhibit a featureless shape with a general decrease in

317 absorbance as the wavelength increases, which is a typical characteristic of HULIS

318 found in rainwater, biomass burning (BB), and ambient aerosols (Huo et al., 2021;

319 Santos et al., 2009; Zhang et al., 2022b). The E_2/E_3 ratio, commonly used as an

320 indicator of the chemical characteristics of organic species, is inversely correlated

321 with higher aromaticity and larger molecular weight (Fan et al., 2021; Li et al., 2022;

322 Sun et al., 2021). As listed in Table 1, the E_2/E_3 of HMW HULIS fractions generally

323 were lower than that of LMW HULIS in both ambient aerosols. This is consistent

324 with the expectation that larger-sized HULIS generally possess more polyconjugated

325 and polymeric structures (Fan et al., 2021; Zhang et al., 2022c), leading to greater

326 aromaticity and larger molecular size.

327   MAE_{365} and AAE are commonly used to characterize the light absorption

328 capacity and the spectral dependence of light absorption by aerosol chromophores,

329 respectively (Bao et al., 2022; Fan et al., 2016b; Kumar et al., 2017; Yuan et al., 2021;

330 Zou et al., 2020). As listed in Table 1, the average MAE_{365} values of HMW HULIS

331 are 0.23 and 1.06 m^2 g^{-1} in summer and winter aerosol, respectively. These values are

332 higher than the corresponding values of 0.20 and 0.88 m^2 g^{-1}, respectively, for LMW

333 HULIS. In addition, HMW HULIS presented lower AAE values, being 7.59 and 6.25

334 in summer and winter aerosol, respectively, than the corresponding values of 8.25 and

335 7.28, respectively, for LMW HULIS (Table 1). These findings are consistent with the

observation in our previous study that larger WSOM generally own higher MAE_{365} but smaller AAE values than smaller WSOM (Fan et al., 2021). Generally, the results suggest that HMW HULIS exhibit stronger light-absorbing ability but with light absorption showing a weaker wavelength dependence. It is worth noting that combustion sources, such as BB and coal combustion, usually emit primary HULIS with high MAE_{365} values due to the enrichment of poly-aromatic and unsaturated species (Cao et al., 2021; Fan et al., 2018; Huo et al., 2021; Zhang et al., 2021), but with small molecular weight distributions (Di Lorenzo et al., 2018; Di Lorenzo et al., 2017; Wong et al., 2017). Furthermore, subsequent pronounced photooxidation and photobleaching processes can lead to a enrichment and/or formation of large sized chromophores (Di Lorenzo et al., 2018; Di Lorenzo et al., 2017; Wong et al., 2017), concurrently resulting in a reduction in their absorption capacity and an enhancement of their spectra dependence on wavelength (Chen et al., 2021b; Fan et al., 2019; Wu et al., 2018; Wu et al., 2020; Zhang et al., 2022a). From this perspective, the SOA formation might induce the generation of HMW HULIS with lower light absorption capacity and weaker light absorption wavelength dependence. In contrast, LMW HULIS is more likely to represent small-sized primary HULIS and/or by-products resulting from the degradation and oxidation of primary large-sized HULIS. Considering the complex sources of ambient HULIS, future studies should explore the MW-dependent light absorption characteristics of HULIS from different sources.

3.2.2. Fluorescence characteristics

The EEM contours of MW HULIS fractions from both summer and winter aerosols are presented in Fig. S4. These HULIS fractions from both seasons exhibit similar EEM spectra features, with a predominance of humic-like fluorophores (Ex/Em = 210-235/395-410 nm). This observation suggest that humic-like fluorophores are fundamental constituents of both HMW and LMW HULIS, which are consistent with previous findings for aerosols MW WSOM (Fan et al., 2021) and bulk HULIS in BB-derived and ambient aerosols (Fan et al., 2020; Qin et al., 2018). The findings imply an assembly of small and heterogeneous molecules to form bulk HULIS through weak intramolecular forces (i.e., π–π, van der Waals, hydrophobic, or hydrogen bonds) (Fan et al., 2021; Piccolo, 2002) and/or charge-transfer interactions (Phillips et al., 2017; Qin et al., 2022). In this study, the fluorescence regional integration (FRI) method was applied to characterize the fluorescent composition of MW HULIS. Using FRI, EEM spectra were divided into five fluorescence regions (labeled as I to V) (Fig. S4), which were successively assigned to simple aromatic proteins (I and II), fulvic acid-like (III), soluble microbial byproduct-like (IV), and humic acid-like (V) substances, respectively, as established in previous studies (Chen et al., 2003; Qin et al., 2018; Wang et al., 2021b). As shown in Fig. S5, the large-size aromatic proteins (II) and fulvic acid-like substances (III) dominated the fluorophores within MW HULIS in both summer and winter aerosols, comprising approximately 62-64% of the total fluorescence intensity. This finding is consistent with previous reports on bulk HULIS in summer and winter aerosols from industrial and urban cities (Qin et al., 2018; Wang et al., 2021b). In comparison, the HMW HULIS in both

summer and winter aerosols generally exhibited a higher proportion of humic

acid-like substances (V), while having a lower abundance of small-size aromatic

proteins I compared to LMW HULIS. These differences are particularly pronounced

in winter aerosols, with the humic acid-like substances accounting for 23% in HMW

HULIS compared to 13% in LMW HULIS, and small-size aromatic proteins I

comprising 9% in HMW HULIS compared to 17% in LMW HULIS (Fig. S5).

Furthermore, the higher HIX values of HMW HULIS (5.64) in comparison to LMW

HULIS (1.94) further support these differences (Table 1). The pronounced BB

emissions and potential NO_2-related oxidation of OA, as evidenced by the presence of

more hotspots (Fig. S1) and higher concentration of NO_2 (Table S1), are likely driving

these marked distinctions between HMW and LMW HULIS in winter aerosols. In

general, these findings imply that the HMW HULIS have a stronger level of

humification and oxidation, while the LMW HULIS appear to be of a simpler nature

and are more likely associated with fresh emissions (e.g., BB).

3.3 Molecular-level insights into MW HULIS

3.3.1. Seasonal variations in the molecular composition of MW HULIS

The molecular-level characteristics of MW HULIS were examined using

negative ESI- HRMS analysis. It is worth noting that the ESI- HRMS could reveal

molecular composition of a subset of organic molecules that are biased ionized in the

negative ESI source, particularly acid compounds such as carboxylic and sulfonic

acids, and may not represent the entire HULIS composition (He et al., 2023; Lin et al.,

2012). Additionally, HRMS techniques are often known to be biased towards low masses below 600 Da (Lin et al., 2012; Wang et al., 2019), suggesting that the molecular sizes calculated by HRMS are likely underestimated. Fig. 3 displays the reconstructed mass spectra of all HULIS fraction in both summer and winter aerosols. Hundreds of peaks can be observed in the spectra ranging from m/z 100 to 450 for all samples, with most ions being abundant within the m/z 150-350 range. These spectrum characteristics are similar to the low m/z range previously reported for HULIS in ambient aerosols and BB emissions (He et al., 2023; Song et al., 2022; Sun et al., 2021; Wang et al., 2019; Zhang et al., 2021; Zou et al., 2023). The similarity in low m/z range among HMW and LMW HULIS and other bulk HULIS may indicate their shared fundamental molecules, further suggesting the potential disassembly of larger molecules.
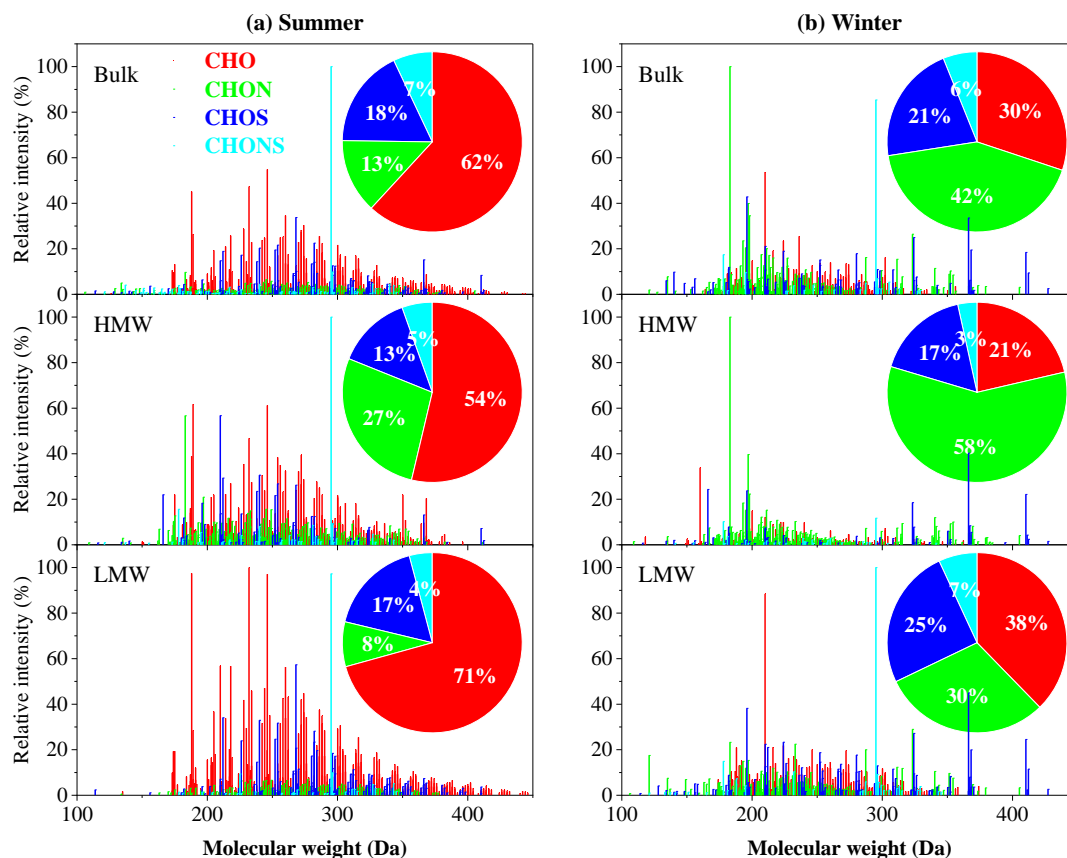
Fig. 3. Mass spectra of bulk and MW HULIS in (a) summer and (b) winter aerosols. The pie charts represent the intensity distributions of four compound categories (CHO, CHON, CHOS, and CHONS).

As listed in Table 2, the number of assigned formulas within MW HULIS in summer aerosols were 655-672, which was higher than the range of 470-506 observed in winter aerosols. This suggests that the MW HULIS in summer aerosols exhibited greater diversity than those in winter aerosols, mainly due to the stronger SOA formation that enhanced the heterogeneity of HULIS fractions in the summer. Moreover, SOA-derived HULIS generally contain more polar molecules (e.g., -OH, -COOH) (Di Lorenzo et al., 2017; Fan et al., 2020; Huo et al., 2021), making them more susceptible to deprotonation and leading to the generation of a greater number

427 formulas under negative ESI conditions. The identified formulas were then classified

428 into four groups (i.e., CHO, CHON, CHOS and CHONS) according to their elemental

429 composition. As depicted in pie charts in Fig. 3, summer HULISs are predominantly

430 composed of CHO (54-71%), while winter HULISs feature a high concentration of

431 both CHON (30-58%) and CHO (21-38%). The notably higher content of CHO in

432 summer HULISs are likely due to a wide distribution of biogenic VOC-derived SOAs

433 during the summer season (Li et al., 2022; Sun et al., 2023). CHON content in winter

434 HULISs is generally higher than in summer ones, potentially due to more significant

435 contributions from direct BB, as well as secondary nitrogen-related chemical

436 processes during the winter season (He et al., 2023; Song et al., 2022; Zhang et al.,

437 2021; Zou et al., 2023). This finding is supported by the greater number of fire spots

438 (Fig. S1) and higher concentrations of NO_2 (Table S1) during winter. The higher

439 proportions of CHON compounds in aerosol HULIS typically lead to enhanced light

440 absorption capabilities (He et al., 2023; Song et al., 2022; Zeng et al., 2021). This

441 provides a potential explanation for the higher MAE_{365} values observed in winter

442 HULIS compared to summer HULIS. Additionally, CHOS is more abundant in winter

443 HULISs (17-25%) than in summer aerosols (13-18%). Previous studies have

444 demonstrated that both coal combustion and the oxidation initiated by SO_2 can lead to

445 the generation of larger amounts of S-containing compounds (Song et al., 2018; Song

446 et al., 2022; Zou et al., 2023). This finding suggested that the increased levels of coal

447 combustion and SO_2-related SOAs, as evidenced by higher concentration of SO_2

448 (Table S1), are significant contributors to the presence of BrC in winter compared to

449   in summer.

Table 2. The average values of intensity-weighted molecular weights (MW), elemental ratios, double bond equivalents (DBE), modified

aromaticity index (AI_{mod}) and carbon oxidation state (OS_C) for tentatively identified compounds of the bulk and MW HULIS samples.

		Elemental compositions	Number of formulas	MW_w	H/C_w	O/C_w	N/C_w	S/C_w	O/N_w	O/S_w	OM/OC_w	DBE_w	DBE/C_w	$DBE\text{-}O_w$	$AI_{mod,w}$	$OS_{C,w}$
Summer	BULK	CHO	376	276	1.39	0.59					1.91	4.69	0.39	-2.20	0.15	-0.21
		CHON	270	260	1.35	0.60	0.15		5.52		2.10	4.99	0.50	-1.17	0.27	-0.14
		CHOS	133	278	1.74	0.71		0.11		6.61	2.38	2.21	0.24	-4.41	0.02	-0.33
		CHONS	81	265	1.69	0.59	0.18	0.14	4.98	5.20	2.49	3.38	0.36	-1.95	0.09	-0.52
		Total	860	273	1.47	0.61	0.03	0.03	1.09	1.54	2.06	4.20	0.38	-2.44	0.14	-0.24
	HMW	CHO	270	264	1.41	0.55					1.85	4.51	0.38	-1.70	0.16	-0.32
		CHON	264	248	1.42	0.61	0.14		5.23		2.09	4.44	0.47	-1.33	0.24	-0.20
		CHOS	72	247	1.82	0.75		0.14		5.83	2.53	1.81	0.22	-4.07	0.01	-0.32
		CHONS	39	269	1.55	0.64	0.19	0.15	4.87	5.16	2.60	3.82	0.44	-1.65	0.14	-0.28
		Total	645	258	1.48	0.60	0.05	0.03	1.70	1.07	2.05	4.09	0.39	-1.91	0.16	-0.29
	LMW	CHO	365	275	1.34	0.64					1.97	4.82	0.42	-2.47	0.16	-0.05
		CHON	155	272	1.39	0.66	0.11		6.60		2.12	4.80	0.45	-2.09	0.18	-0.08
		CHOS	120	284	1.71	0.74		0.11		7.05	2.43	2.51	0.25	-4.58	0.02	-0.22
		CHONS	32	322	1.71	0.64	0.11	0.11	6.59	6.63	2.42	3.32	0.30	-3.41	0.06	-0.42
		Total	672	278	1.42	0.66	0.01	0.02	0.80	1.48	2.08	4.36	0.39	-2.84	0.13	-0.10
Winter	BULK	CHO	142	247	1.23	0.48					1.75	5.35	0.47	-0.05	0.32	-0.26
		CHON	194	231	1.24	0.53	0.16		3.96		1.99	5.17	0.57	0.52	0.48	-0.18
		CHOS	79	271	1.93	0.51		0.11		4.97	2.14	1.21	0.14	-3.80	0.04	-0.91
		CHONS	20	271	1.61	0.69	0.16	0.13	5.60	5.90	2.60	3.32	0.40	-2.65	0.09	-0.24
		Total	435	247	1.41	0.52	0.08	0.03	2.02	1.42	1.99	4.27	0.44	-0.77	0.31	-0.37
	HMW	CHO	138	232	1.36	0.47					1.74	4.79	0.41	0.02	0.28	-0.42

	CHON	244	232	1.29	0.53	0.16		3.89		2.01	4.87	0.55	0.23	0.44	-0.23
	CHOS	59	292	2.08	0.40		0.12		4.40	2.04	0.46	0.06	-4.06	0.02	-1.27
	CHONS	29	236	1.74	0.48	0.22	0.20	2.82	3.02	2.57	2.88	0.38	-0.57	0.27	-0.77
	Total	470	242	1.46	0.50	0.10	0.03	2.37	0.85	1.98	4.04	0.43	-0.57	0.33	-0.46
LMW	CHO	176	249	1.23	0.54					1.82	5.25	0.48	-0.65	0.30	-0.15
	CHON	195	239	1.34	0.49	0.16		3.99		1.95	4.88	0.52	0.29	0.45	-0.36
	CHOS	107	280	1.94	0.54		0.10		5.42	2.17	1.20	0.13	-4.25	0.02	-0.85
	CHONS	28	272	1.67	0.69	0.16	0.14	5.89	6.03	2.63	2.99	0.37	-3.15	0.13	-0.29
	Total	506	256	1.47	0.54	0.06	0.04	1.61	1.78	2.01	3.96	0.39	-1.45	0.26	-0.40

452   Table 2 summarizes the intensity-weighted molecular parameters for MW

453   HULIS in both summer and winter aerosols. Evidently, the MWw of summer HULISs

454   are 258-278, which are higher than the corresponding values of 242-256 for winter

455   HULISs. It is noted that these values are considerably smaller than those revealed by

456   HPSEC analysis. This difference could be explained by several factors: (1) ESI-

457   HRMS is biased towards relatively small molecules that easily deprotonated in

458   negative ESI mode (He et al., 2023; Lin et al., 2012); (2) SEC can provide an apparent

459   rather than accurate molecular size of molecules due to the lack of appropriate

460   standards for column calibration (Fan et al., 2023; Wong et al., 2017), and (3) the

461   potential disassembly of larger molecules stabilized by weak forces during

462   electrospray ionization of HRMS (Fan et al., 2021; Phillips et al., 2017). Nevertheless,

463   both HRMS and HPSEC indicate that summer HULISs exhibit larger sizes than

464   winter HULISs. Moreover, summer HULISs exhibit higher O/Cw ranging from 0.60

465   to 0.66, as well as $OS_{C,w}$ ranging from -0.29 to -0.10, which exceed the respective

466   values of 0.50 to 0.54 and -0.46 to -0.37 observed in winter HULISs. Conversely,

467   winter HULISs display higher $AI_{mod,w}$ values (0.26-0.33) than those (0.13-0.16) for

468   summer ones. These findings suggest that summer HULISs are characterized by a

469   high degree of oxidation, while winter HULISs exhibit stronger aromaticity.

470

471   3.3.2. Comparison on molecular composition of HMW and LMW HULIS

472   **CHO compounds.** The CHO compounds are prominent constituents within

473   HULIS fractions, accounting for 54% and 21% in summer and winter HMW HULIS,

respectively, whereas these proportions increase to 71% and 38% in LMW HULIS

(Fig. 3). It is worth noting that CHO compounds that undergo deprotonation in ESI-

mode are likely associated with the presence of carboxyl, carbonyl, alcohol and ester

(Lin et al., 2012; Wang et al., 2018). Moreover, CHO compounds in LMW HULIS

exhibit a higher oxygenation level compared to HMW HULIS, as evidenced by the

higher O/C_w and $OS_{C,w}$ values. As shown in Table 2, the O/C_w for CHO in LMW

HULIS are 0.55-0.64, which are higher than 0.47-0.54 observed in HMW HULIS. In

contrast, the H/C_w for CHO in HMW HULIS were consistently higher than those in

LMW HULIS, with values of 1.41 vs. 1.34 in summer and 1.36 vs. 1.23 in winter

(Table 2). This disparity strongly suggests a higher saturation level of CHO

compounds within HMW HULIS. This conclusion is further corroborated by the

lower DBE_w and $AI_{mod,w}$ observed for CHO in HMW HULIS compared to LMW

HULIS (Table 2). It is known that these values serve as estimations of C=C density

and aromatic and condensed aromatic structures (Song et al., 2022; Zhang et al.,

2021). Taken together, the CHO compounds within HMW HULIS exhibit a more

aliphatic nature but lower aromaticity and oxidation levels when compared to those

within LMW HULIS.

CHON compounds. HMW HULIS fractions consist of a higher proportion of

CHON compounds compared to LMW HULIS, with proportions of 27% vs. 8% in

summer and 58% vs. 30% in winter (Fig. 3). This observation suggests that HMW

HULIS contain a higher content of N-containing components. It is noted that the

LMW HULIS are generally characterized by higher O/N_w values of 6.60 in summer

and 3.99 in winter compared to 5.23 in summer and 3.89 in winter for HMW HULIS. This indicates that the CHON compounds within LMW HULIS are more highly oxidized than those within HMW HULIS. In general, compounds with $O/N \geq 3$ are indicative of oxidized N groups such as nitro ($-NO_2$) or nitrooxy ($-ONO_2$), while compounds with $O/N < 3$ may denote the reduced N-containing functional groups (i.e., amines) (He et al., 2023; Song et al., 2022; Zeng et al., 2021). In this study, a majority of the CHON compounds, comprising 73-85% in summer and 59-64% in winter, exhibited $O/N \geq 3$ in both MW HULIS fractions. This suggests that high concentrations of nitro compounds or organonitrates dominate the CHON compounds (Sun et al., 2023; Wang et al., 2018; Zeng et al., 2021), especially in summer samples, primarily due to the hydroxyl radical oxidation of biogenic or anthropogenic VOC precursors, as well as BB emissions (Song et al., 2022; Sun et al., 2021; Zhang et al., 2021; Zou et al., 2023). Furthermore, the CHON compounds exhibiting $O/N \geq 3$ were more abundant in LMW HULIS compared to HMW HULIS, accounting for 85% vs. 73% in summer and 64% vs. 59% in winter. In contrast, HMW HULIS contained more CHON compounds with $O/N < 3$ compared to LMW HULIS. These findings collectively indicate that the CHON within HMW HULIS possess lower content of nitro compounds or organonitrates than LMW HULIS. Based on FTIR analysis (Text S2 and Fig. S6 in SI), it is known that HMW HULIS contain more carboxylic groups than LMW HULIS, which indicate a higher likelihood of HMW HULIS containing more amino acids.

CHOS and CHONS compounds. In this study, we observed that CHOS

accounted for proportions of 13% to 25% in all MW HULIS fractions, while CHONS

had a lower proportion of 3% to 7% (Fig. 3). Notably, the distribution of CHOS

differed between HMW and LMW HULIS in both season samples. As depicted in Fig.

3, HMW HULIS contained fewer CHOS compounds compared to LMW HULIS, with

proportions of 13% vs. 17% in summer and 17% vs. 25% in winter. This finding

suggests that a greater number of CHOS compounds are incorporated into the LMW

HULIS fractions, which potentially leading to a reduction in the light absorption of

LMW HULIS (Zeng et al., 2021; Zhang et al., 2021). Furthermore, as indicated in

Table 2, both the CHOS and CHONS within LMW HULIS exhibited higher O/Sw

values than HMW HULIS in both seasonal samples. Consequently, the S-containing

compounds within LMW HULIS were characterized by a higher degree of oxidation,

primarily attributed to SO_2-related chemical oxidation process, in comparison to those

in HMW HULIS. Moreover, it was observed that 61% to 92% of CHOS compounds

exhibited O/S > 4, and 3% to 43% of CHONS compounds with O/S > 7 for all MW

HULIS fractions. Among them, HMW HULIS own lower proportions of CHOS with

O/S > 4 and CHONS with O/S > 7 than LMW HULIS, suggesting a reduced presence

of potential organosulfates and nitrooxyorganosulfates within HMW HULIS (Sun et

al., 2023; Wang et al., 2018; Zeng et al., 2021; Zou et al., 2023).

3.3.3. Comparative analysis of unique molecular formulas in HMW and LMW HULIS

In this study, particular emphasis was placed on the unique molecular formulas

540 within the HMW or LMW HULIS fractions. Fig. 4a, b illustrates the Van Krevelen

541 (VK) diagram depicting the distribution of unique molecular formulas within HMW

542 and LMW HULIS in summer and winter samples. It is evident that a majority of

543 unique formulas within LMW HULIS are concentrated around the origin with O/C >

544 0.5, accounting for 83% in summer and 64% in winter. In contrast, most formulas

545 within HMW HULIS exhibited O/C < 0.5, representing about 58% for both seasonal

546 samples. These findings indicate that the unique molecules within LMW HULIS

547 consist of more polar O-containing organic compounds than those within HMW

548 HULIS.

549

550
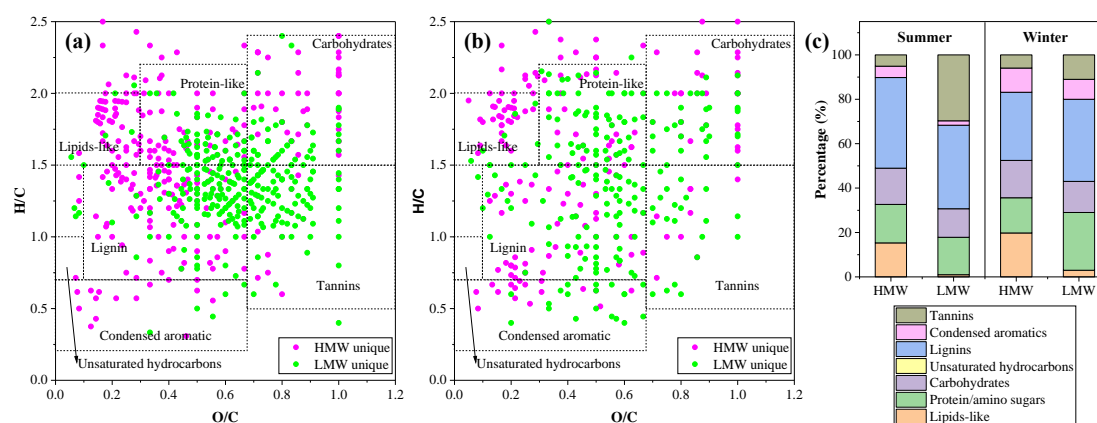
Fig. 4. Van Krevelen diagrams for the unique molecular formulas within HMW and LMW HULIS from (a) summer and (b) winter aerosols. (c) The contributions of major substances classes in unique formulas.

554

555 The molecular formulas are further categorized into seven groups based on

556 previous studies, including lignin-like species, protein/amino sugars, condensed

557 aromatics, tannin-like species, carbohydrate-like species, unsaturated hydrocarbons,

558 and lipid-like species (He et al., 2023; Sun et al., 2021; Sun et al., 2023). The

559 classification rules for these formulas can be found in Table S2. Fig. 4c provides an

560 overview of the relative contributions of the number of unique formulas from each of

561 the seven groups for HMW and LMW HULIS. The results indicate that the dominant

562 substance class in the unique formulas within both MW HULIS are lignin-like species,

563 accounting for proportions of 31-40%. This finding indicates that lignin derivatives

564 are fundamental components in both HMW and LMW HULIS either in summer or

565 winter aerosols. Additionally, there are notable differences in the molecular

566 characteristics of lignin-like species within HMW and LMW HULIS. As listed in

567 Table S3, lignin-like species within HMW HULIS exhibit lower MWw and O/Cw, but

568 higher N/Cw and AImod,w values than those within LMW HULIS in both seasonal

569 samples. These observations suggest that the unique lignin-like substances in HMW

570 HULIS likely contain more N-enriched and highly aromatic species, while those in

571 LMW HULIS tend to concentrate more aliphatic O-containing compounds. These

572 distinctions in composition and characteristics between HMW and LMW HULIS

573 fractions provide valuable insights into their origins and transformations in the

574 atmosphere.

575 Moreover, there are notable variations in the contributions of lipids-like,

576 protein/amino sugars, carbohydrates, condensed aromatics, and tannins species

577 between HMW and LMW HULIS. In general, HMW HULIS have a higher proportion

578 of lipids-like species, carbohydrates and condensed aromatics than LMW HULIS in

579 both summer and winter aerosols. Among these, the most remarkable difference in

580 composition between HMW HULIS and LMW HULIS is seen in lipids-like species,

581 accounting for 15% versus 1% in summer and 20% versus 3% in winter (Fig. 4). As

582 reported in previous studies, lipids-like species primarily originate from biogenic

583 emissions (He et al., 2023; Li et al., 2022; Sun et al., 2021). This suggests that there is

584 a stronger contribution from biogenic emissions to HMW HULIS. Additionally, these

585 species in HMW HULIS were usually characterized by lower DBE_w and slightly

586 lower $OS_{C,w}$ when compared to LMW HULIS (Table S3), indicating they present

587 stronger saturation and fewer oxidized substituents. On the other hand, tannins species

588 contribute a higher proportion to LMW HULIS, constituting 30% in summer and 11%

589 in winter, while comprising only 5%-6% in HMW HULIS in both season aerosols.

590 Tannin-like species are known to consist of various polyphenolic groups containing

591 hydroxyl and carboxylic functional groups (He et al., 2023; Li et al., 2022; Ning et al.,

592 2019; Sun et al., 2021). The slightly lower DBE_w but much higher $DBE\text{-}O_w$ for

593 unique tannin-like species within HMW HULIS were observed compared to LMW

594 HULIS (Table S3), suggesting that the former ones are enriched in more unsaturated

595 O-containing functional groups, particularly carboxylic functional groups.

596

597 3.4. Atmospheric implications

598   This study provides comprehensive comparison between HMW and LMW

599 HULIS regarding their distributions, chemical structures, molecular sizes and

600 compositions. HMW HULIS appear to be larger than LMW HULIS, as evidenced by

601 both ultrafiltration natures and the MW distributions of chromophores analyzed by

602 HPSEC. However, HRMS analysis revealed that the average MWw of identified

603 formulas within HMW HULIS were lower than those of LMW HULIS (Table 2). This

604 discrepancy can likely be attributed to the "assembled structures" that construct the

605 aerosol HULIS, as suggested in many previous studies focusing on HULIS and BrC

606 characterization (Fan et al., 2021; Fan et al., 2023; Phillips et al., 2017; Qin et al.,

607 2022). In fact, the results from EEM-FRI and FTIR analysis support the notion that

608 HMW and LMW HULIS likely consist of potential structures assembled by similar

609 basic fluorophores and functional groups. Based on this theory, HMW HULIS may

610 consist of macromolecular species primarily assembled from small molecules through

611 weak forces (i.e., π–π, van der Waals, hydrophobic, or hydrogen bonds) and/or

612 charge-transfer interactions (Fan et al., 2021; Phillips et al., 2017), which can

613 potentially disassemble during ESI ionization and form low MW molecules.

614   Based on the molecular-level characterization, significant distinctions in

615 properties between HMW HULIS and LMW HULIS become evident. HMW HULIS

616 generally exhibit stronger aromaticity but lower oxidation degree when compared to

617 LMW HULIS. In terms of molecular composition, HMW HULIS contain higher

618 quantities of CHON species but lower quantities of CHO compounds than LMW

619 HULIS. Furthermore, more lipids-like species were identified as unique molecules in

620 HMW HULIS, while more tannin-like species with abundant carboxylic groups were

621 observed as unique molecules in LMW HULIS. Given these pronounced differences

622 between HMW and LMW HULIS, it can be speculated that the higher levels of

623 aromatic structures, greater presence of CHON molecules and the presence of

624 lipids-like species may serve as driving factors in the formation of potential

assembled structures in HMW HULIS. Additionally, it is well-established that CHON can enhance the light absorption of organic aerosols (OA), while CHO species may have the opposite effect, weakening light absorption (He et al., 2023; Song et al., 2022; Wang et al., 2019; Zeng et al., 2021). Therefore, it is reasonable to conclude that HMW HULIS possess stronger light absorbing capability, which is consistent with their larger MAE_{365} values.

Importantly, HMW HULIS contain higher amounts of carboxylic functional groups, reduced nitrogen species (e.g., amines) and aromatic species than LMW HULIS. These functional groups have strong complexation abilities with transition metals (Wang et al., 2021a; Wang et al., 2021b), thus influencing the transformation and chemical behavior of metals. Moreover, the OA-metals complex can potentially enhance the catalytic generation of reactive oxygen species (ROS) in organic aerosols (Win et al., 2018; Zhang et al., 2022a), thereby playing significant roles in adverse health effects of OA. These results reinforce the significance of HMW HULIS in light absorption, metal complexation, and the potential ROS generation ability of aerosol BrC.

4. Conclusions

This study successfully isolated and characterized HMW and LMW HULIS in atmospheric aerosols using the UF-SPE technique, yielding insights into their distribution, optical properties and molecular-level characteristics. Both HMW and LMW HULIS exhibited a continuum of MW distributions ranging from 100 to 20,000

Da. However, HMW HULIS displayed more extensive and intricate MW distributions, suggesting differences in their sources and formation processes compared to LMW HULIS. In general, HMW HULIS constituted a higher percentage of TOC and UV254 in aerosols compared to LMW HULIS, indicating the prevalence of hydrophobic and conjugated aromatic structures in the former. Moreover, HMW HULIS exhibited higher aromaticity, stronger light absorption abilities, weaker spectra dependence, and stronger humification and conjugation, compared to LMW HULIS. Interestingly, HRMS analysis revealed slightly lower MWw values for HMW HULIS than LMW HULIS, which contradicted the HPSEC results and the nature of UF fractionation. This finding strongly suggests the possibility of small molecules assembling to form macromolecules in HMW HULIS. Regarding molecular composition, HMW HULIS contained a higher proportion of CHON compounds, constituting 27% vs. 8% in summer and 58% vs. 30% in winter, while LMW HULIS were primarily composed of CHO compounds, accounting for 71% vs. 54%% in summer and 38% vs. 21% in winter. Both HMW and LMW HULIS featured lignin-like substances as major unique molecular formulas, but HMW HULIS exhibited more N-enriched and highly aromatic species, whereas LMW HULIS contained a higher proportion of polar O-containing functional groups. Additionally, HMW HULIS included a greater number of unique lipids-like compounds, while LMW HULIS tend to concentrate more tannin-like compounds. These observations shed light on the complex nature of MW HULIS, and their diverse sources and transformations. Future research should expand the geographical and seasonal coverage to gain a more comprehensive

understanding of the molecular-level characteristics of MW HULIS in various atmospheric environments. Furthermore, exploring additional physicochemical properties of MW HULIS will provide valuable insights into their potential health and environmental implications. Overall, this study offers valuable insights into the molecular-level characteristics of aerosol HULIS, enhancing our understanding of their evolution, sources and potential environmental effects.

Author contribution

Xingjun Fan: Methodology, Supervision, Funding acquisition, Writing-review & editing. **Ao Cheng:** Sampling, Data curation. **Xufang Yu:** Writing-review & editing. **Tao Cao:** Sampling, Investigation. **Dan Chen:** Investigation, Data curation. **Wenchao Ji:** Formal analysis. **Yongbing Cai:** Writing-review & editing. **Fande Meng:** Writing-review & editing. **Jianzhong Song:** Methodology, Writing-review & editing. **Pingan Peng:** Writing-review & editing.

Declaration of Competing Interest

The authors declare that they have no known competing financial interests or personal relationships that could have appeared to influence the work reported in this paper.

Acknowledgments

This study was supported by the Natural Science Foundation of China (42192514, 52100114), the Anhui Provincial Natural Science Foundation (2108085MD140, 2108085QB56), and the State key Laboratory of Organic Geochemistry, GIGCAS (SKLOG202101), Anhui Provincial Key Science Foundation for Outstanding Young

691   Talent (2022AH030145, gxyqZD2021126).

692

693   **References**

694   Bao, M., Zhang, Y.-L., Cao, F., Lin, Y.-C., Hong, Y., Fan, M., Zhang, Y., Yang, X., Xie, F., 2022. Light
695   absorption and source apportionment of water soluble humic-like substances (HULIS) in
696   PM2.5 at Nanjing, China. Environmental Research 206, 112554.
697   Birdwell, J.E., Valsaraj, K.T., 2010. Characterization of dissolved organic matter in fogwater by
698   excitation–emission matrix fluorescence spectroscopy. Atmos. Environ. 44, 3246-3253.
699   Cao, T., Li, M., Xu, C., Song, J., Fan, X., Li, J., Jia, W., Peng, P., 2022. Technical note: Identification of
700   chemical composition and source of fluorescent components in atmospheric
701   water-soluble brown carbon by excitation-emission matrix with parallel factor analysis:
702   Potential limitation and application. Atmos. Chem. Phys. Discuss. 2022, 1-41.
703   Cao, T., Li, M., Zou, C., Fan, X., Song, J., Jia, W., Yu, C., Yu, Z., Peng, P., 2021. Chemical composition,
704   optical properties, and oxidative potential of water- and methanol-soluble organic
705   compounds emitted from the combustion of biomass materials and coal. Atmos. Chem.
706   Phys. 21, 13187-13205.
707   Chen, J., Wu, Z.J., Zhao, X., Wang, Y.J., Chen, J.C., Qiu, Y.T., Zong, T.M., Chen, H.X., Wang, B.B., Lin,
708   P., Liu, W., Guo, S., Yao, M.S., Zeng, L.M., Wex, H., Liu, X., Hu, M., Li, S.M., 2021a.
709   Atmospheric Humic-Like Substances (HULIS) Act as Ice Active Entities. Geophysical
710   Research Letters 48, e2021GL092443.
711   Chen, Q., Hua, X., Dyussenova, A., 2021b. Evolution of the chromophore aerosols and its driving
712   factors in summertime Xi'an, Northwest China. Chemosphere 281, 130838.
713   Chen, W., Westerhoff, P., Leenheer, J.A., Booksh, K., 2003. Fluorescence Excitation-Emission
714   Matrix Regional Integration to Quantify Spectra for Dissolved Organic Matter. Environ.
715   Sci. Technol. 37, 5701-5710.
716   Di Lorenzo, R.A., Place, B.K., VandenBoer, T.C., Young, C.J., 2018. Composition of Size-Resolved
717   Aged Boreal Fire Aerosols: Brown Carbon, Biomass Burning Tracers, and Reduced
718   Nitrogen. ACS Earth and Space Chemistry 2, 278-285.
719   Di Lorenzo, R.A., Washenfelder, R.A., Attwood, A.R., Guo, H., Xu, L., Ng, N.L., Weber, R.J., Baumann,
720   K., Edgerton, E., Young, C.J., 2017. Molecular-Size-Separated Brown Carbon Absorption
721   for Biomass-Burning Aerosol at Multiple Field Sites. Environ. Sci. Technol. 51, 3128-3137.
722   Dinar, E., Taraniuk, I., Graber, E.R., Anttila, T., Mentel, T.F., Rudich, Y., 2007. Hygroscopic growth of
723   atmospheric and model humic-like substances. J.Geophys. Res. 112.
724   Fan, X., Cai, F., Xu, C., Yu, X., Wang, Y., Xiao, X., Ji, W., Cao, T., Song, J., Peng, P.a., 2021. Molecular
725   weight-dependent abundance, absorption, and fluorescence characteristics of
726   water-soluble organic matter in atmospheric aerosols. Atmos. Environ. 247.
727   Fan, X., Cao, T., Yu, X., Wang, Y., Xiao, X., Li, F., Xie, Y., Ji, W., Song, J., Peng, P., 2020. The
728   evolutionary behavior of chromophoric brown carbon during ozone aging of fine
729   particles from biomass burning. Atmos. Chem. Phys. 20, 4593-4605.
730   Fan, X., Cheng, A., Chen, D., Cao, T., Ji, W., Song, J., Peng, P., 2023. Investigating the molecular
731   weight distribution of atmospheric water-soluble brown carbon using high-performance

732   size exclusion chromatography coupled with diode array and fluorescence detectors.
733   Chemosphere 338, 139517.

734 Fan, X., Li, M., Cao, T., Cheng, C., Li, F., Xie, Y., Wei, S., Song, J., Peng, P.a., 2018. Optical properties
735   and oxidative potential of water- and alkaline-soluble brown carbon in smoke particles
736   emitted from laboratory simulated biomass burning. Atmos. Environ. 194, 48-57.

737 Fan, X., Song, J., Peng, P., 2013. Comparative study for separation of atmospheric humic-like
738   substance (HULIS) by ENVI-18, HLB, XAD-8 and DEAE sorbents: elemental composition,
739   FT-IR, 1H NMR and off-line thermochemolysis with tetramethylammonium hydroxide
740   (TMAH). Chemosphere 93, 1710-1719.

741 Fan, X., Song, J., Peng, P.a., 2016a. Temporal variations of the abundance and optical properties
742   of water soluble Humic-Like Substances (HULIS) in PM2.5 at Guangzhou, China. Atmos.
743   Res. 172–173, 8-15.

744 Fan, X., Wei, S., Zhu, M., Song, J., Peng, P., 2016b. Comprehensive characterization of humic-like
745   substances in smoke PM2.5 emitted from the combustion of biomass materials and fossil
746   fuels. Atmos. Chem. Phys. 16, 13321-13340.

747 Fan, X., Yu, X., Wang, Y., Xiao, X., Li, F., Xie, Y., Wei, S., Song, J., Peng, P.a., 2019. The aging
748   behaviors of chromophoric biomass burning brown carbon during dark aqueous
749   hydroxyl radical oxidation processes in laboratory studies. Atmos. Environ. 205, 9-18.

750 Fan, X.J., Song, J.Z., Peng, P.A., 2012. Comparison of isolation and quantification methods to
751   measure humic-like substances (HULIS) in atmospheric particles. Atmos. Environ. 60,
752   366-374.

753 Graber, E.R., Rudich, Y., 2006. Atmospheric HULIS: How humic-like are they? A comprehensive
754   and critical review. Atmos. Chem. Phys. 6, 729-753.

755 He, T., Wu, Y., Wang, D., Cai, J., Song, J., Yu, Z., Zeng, X., Peng, P.a., 2023. Molecular compositions
756   and optical properties of water-soluble brown carbon during the autumn and winter in
757   Guangzhou, China. Atmos. Environ. 296, 119573.

758 Huo, Y., Wang, Y., Qi, W., Jiang, M., Li, M., 2021. Comprehensive characterizations of HULIS in
759   fresh and secondary emissions of crop straw burning. Atmos. Environ. 248, 118220.

760 Kawasaki, N., Matsushige, K., Komatsu, K., Kohzu, A., Nara, F.W., Ogishi, F., Yahata, M., Mikami, H.,
761   Goto, T., Imai, A., 2011. Fast and precise method for HPLC–size exclusion
762   chromatography with UV and TOC (NDIR) detection: Importance of multiple detectors to
763   evaluate the characteristics of dissolved organic matter. Water Res. 45, 6240-6248.

764 Kumar, V., Goel, A., Rajput, P., 2017. Compositional and surface characterization of HULIS by
765   UV-Vis, FTIR, NMR and XPS: Wintertime study in Northern India. Atmos. Environ. 164,
766   468-475.

767 Li, X., Yu, F., Cao, J., Fu, P., Hua, X., Chen, Q., Li, J., Guan, D., Tripathee, L., Chen, Q., Wang, Y., 2022.
768   Chromophoric dissolved organic carbon cycle and its molecular compositions and
769   optical properties in precipitation in the Guanzhong basin, China. Sci. Total Environ. 814,
770   152775.

771 Lin, P., Rincon, A.G., Kalberer, M., Yu, J.Z., 2012. Elemental composition of HULIS in the Pearl River
772   Delta Region, China: results inferred from positive and negative electrospray high
773   resolution mass spectrometric data. Environ. Sci. Technol. 46, 7454-7462.

774 Ma, Y., Cheng, Y., Qiu, X., Cao, G., Kuang, B., Yu, J.Z., Hu, D., 2019. Optical properties, source
775   apportionment and redox activity of humic-like substances (HULIS) in airborne fine

776   particulates in Hong Kong. Environmental Pollution 255, 113087.

777 Mukherjee, A., Dey, S., Rana, A., Jia, S., Banerjee, S., Sarkar, S., 2020. Sources and atmospheric
778   processing of brown carbon and HULIS in the Indo-Gangetic Plain: Insights from
779   compositional analysis. Environmental Pollution 267, 115440.

780 Ning, C., Gao, Y., Zhang, H., Yu, H., Wang, L., Geng, N., Cao, R., Chen, J., 2019. Molecular
781   characterization of dissolved organic matters in winter atmospheric fine particulate
782   matters (PM2.5) from a coastal city of northeast China. Sci. Total Environ. 689, 312-321.

783 Phillips, S.M., Bellcross, A.D., Smith, G.D., 2017. Light Absorption by Brown Carbon in the
784   Southeastern United States is pH-dependent. Environ. Sci. Technol. 51, 6782-6790.

785 Piccolo, A., 2002. The supramolecular structure of humic substances: A novel understanding of
786   humus chemistry and implications in soil science, Advances in Agronomy. Academic
787   Press, pp. 57-134.

788 Qin, J., Zhang, L., Qin, Y., Shi, S., Li, J., Gao, Y., Tan, J., Wang, X., 2022. pH-Dependent Chemical
789   Transformations of Humic-Like Substances and Further Cognitions Revealed by Optical
790   Methods. Environ. Sci. Technol. 56, 7578-7587.

791 Qin, J., Zhang, L., Zhou, X., Duan, J., Mu, S., Xiao, K., Hu, J., Tan, J., 2018. Fluorescence
792   fingerprinting properties for exploring water-soluble organic compounds in PM 2.5 in an
793   industrial city of northwest China. Atmos. Environ. 184, 203-211.

794 Santos, P.S.M., Otero, M., Duarte, R.M.B.O., Duarte, A.C., 2009. Spectroscopic characterization of
795   dissolved organic matter isolated from rainwater. Chemosphere 74, 1053-1061.

796 Santos, P.S.M., Santos, E.B.H., Duarte, A.C., 2012. First spectroscopic study on the structural
797   features of dissolved organic matter isolated from rainwater in different seasons. Sci.
798   Total Environ. 426, 172-179.

799 Song, J., Li, M., Jiang, B., Wei, S., Fan, X., Peng, P., 2018. Molecular Characterization of
800   Water-Soluble Humic like Substances in Smoke Particles Emitted from Combustion of
801   Biomass Materials and Coal Using Ultrahigh-Resolution Electrospray Ionization Fourier
802   Transform Ion Cyclotron Resonance Mass Spectrometry. Environ. Sci. Technol. 52,
803   2575-2585.

804 Song, J., Li, M., Zou, C., Cao, T., Fan, X., Jiang, B., Yu, Z., Jia, W., Peng, P.a., 2022. Molecular
805   Characterization of Nitrogen-Containing Compounds in Humic-like Substances Emitted
806   from Biomass Burning and Coal Combustion. Environ. Sci. Technol. 56, 119-130.

807 Song, J.Z., Huang, W.L., Peng, P.A., Xiao, B.H., Ma, Y.J., 2010. Humic Acid Molecular Weight
808   Estimation by High-Performance Size-Exclusion Chromatography with Ultraviolet
809   Absorbance Detection and Refractive Index Detection. Soil. Sci. Soc. Am. J. 74,
810   2013-2020.

811 Sun, H., Li, X., Zhu, C., Huo, Y., Zhu, Z., Wei, Y., Yao, L., Xiao, H., Chen, J., 2021. Molecular
812   composition and optical property of humic-like substances (HULIS) in winter-time PM2.5
813   in the rural area of North China Plain. Atmos. Environ. 252, 118316.

814 Sun, H., Wu, Z., Kang, X., Zhu, C., Yu, L., Li, R., Lin, Z., Chen, J., 2023. Molecular characterization of
815   humic-like substances (HULIS) in atmospheric particles (PM2.5) in offshore Eastern China
816   Sea (OECS) using solid-phase extraction coupled with ESI FT-ICR MS. Atmos. Environ.
817   294, 119523.

818 Wang, K., Zhang, Y., Huang, R.-J., Cao, J., Hoffmann, T., 2018. UHPLC-Orbitrap mass
819   spectrometric characterization of organic aerosol from a central European city (Mainz,

820   Germany) and a Chinese megacity (Beijing). Atmos. Environ. 189, 22-29.

821   Wang, X., Qin, Y., Qin, J., Long, X., Qi, T., Chen, R., Xiao, K., Tan, J., 2021a. Spectroscopic insight
822   into the pH-dependent interactions between atmospheric heavy metals (Cu and Zn) and
823   water-soluble organic compounds in PM2.5. Sci. Total Environ. 767, 145261.

824   Wang, X.B., Qin, Y.Y., Qin, J.J., Yang, Y.R., Qi, T., Chen, R.Z., Tan, J.H., Xiao, K., 2021b. The
825   interaction laws of atmospheric heavy metal ions and water-soluble organic compounds
826   in PM2.5 based on the excitation-emission matrix fluorescence spectroscopy. Journal of
827   Hazardous Materials 402, 8.

828   Wang, Y., Hu, M., Lin, P., Tan, T., Li, M., Xu, N., Zheng, J., Du, Z., Qin, Y., Wu, Y., Lu, S., Song, Y., Wu,
829   Z., Guo, S., Zeng, L., Huang, X., He, L., 2019. Enhancement in Particulate Organic Nitrogen
830   and Light Absorption of Humic-Like Substances over Tibetan Plateau Due to
831   Long-Range Transported Biomass Burning Emissions. Environ. Sci. Technol. 53,
832   14222-14232.

833   Win, M.S., Tian, Z., Zhao, H., Xiao, K., Peng, J., Shang, Y., Wu, M., Xiu, G., Lu, S., Yonemochi, S.,
834   Wang, Q., 2018. Atmospheric HULIS and its ability to mediate the reactive oxygen
835   species (ROS): A review. J Environ Sci (China) 71, 13-31.

836   Wong, J.P.S., Nenes, A., Weber, R.J., 2017. Changes in Light Absorptivity of Molecular Weight
837   Separated Brown Carbon Due to Photolytic Aging. Environ. Sci. Technol. 51, 8414-8421.

838   Wong, J.P.S., Tsagkaraki, M., Tsiodra, I., Mihalopoulos, N., Violaki, K., Kanakidou, M., Sciare, J.,
839   Nenes, A., Weber, R.J., 2019. Atmospheric evolution of molecular-weight-separated
840   brown carbon from biomass burning. Atmos. Chem. Phys. 19, 7319-7334.

841   Wu, G., Fu, P., Ram, K., Song, J., Chen, Q., Kawamura, K., Wan, X., Kang, S., Wang, X., Laskin, A.,
842   Cong, Z., 2021. Fluorescence characteristics of water-soluble organic carbon in
843   atmospheric aerosol☆. Environmental Pollution 268, 115906.

844   Wu, G., Wan, X., Gao, S., Fu, P., Yin, Y., Li, G., Zhang, G., Kang, S., Ram, K., Cong, Z., 2018.
845   Humic-Like Substances (HULIS) in Aerosols of Central Tibetan Plateau (Nam Co, 4730 m
846   asl): Abundance, Light Absorption Properties, and Sources. Environ. Sci. Technol. 52,
847   7203-7211.

848   Wu, G., Wan, X., Ram, K., Li, P., Liu, B., Yin, Y., Fu, P., Loewen, M., Gao, S., Kang, S., Kawamura, K.,
849   Wang, Y., Cong, Z., 2020. Light absorption, fluorescence properties and sources of brown
850   carbon aerosols in the Southeast Tibetan Plateau. Environmental Pollution 257, 113616.

851   Yuan, W., Huang, R.-J., Yang, L., Ni, H., Wang, T., Cao, W., Duan, J., Guo, J., Huang, H., Hoffmann,
852   T., 2021. Concentrations, optical properties and sources of humic-like substances (HULIS)
853   in fine particulate matter in Xi'an, Northwest China. Sci. Total Environ. 789, 147902.

854   Zeng, Y., Ning, Y., Shen, Z., Zhang, L., Zhang, T., Lei, Y., Zhang, Q., Li, G., Xu, H., Ho, S.S.H., Cao, J.,
855   2021. The Roles of N, S, and O in Molecular Absorption Features of Brown Carbon in
856   PM2.5 in a Typical Semi-Arid Megacity in Northwestern China. Journal of Geophysical
857   Research: Atmospheres 126, e2021JD034791.

858   Zhang, T., Huang, S., Wang, D., Sun, J., Zhang, Q., Xu, H., Hang Ho, S.S., Cao, J., Shen, Z., 2022a.
859   Seasonal and diurnal variation of PM2.5 HULIS over Xi'an in Northwest China: Optical
860   properties, chemical functional group, and relationship with reactive oxygen species
861   (ROS). Atmos. Environ. 268, 118782.

862   Zhang, T., Shen, Z., Huang, S., Lei, Y., Zeng, Y., Sun, J., Zhang, Q., Ho, S.S.H., Xu, H., Cao, J., 2022b.
863   Optical properties, molecular characterizations, and oxidative potentials of different

864   polarity levels of water-soluble organic matters in winter PM2.5 in six China's megacities.
865   Sci. Total Environ. 853, 158600.

866 Zhang, T., Shen, Z., Zeng, Y., Cheng, C., Wang, D., Zhang, Q., Lei, Y., Zhang, Y., Sun, J., Xu, H., Ho,
867   S.S.H., Cao, J., 2021. Light absorption properties and molecular profiles of HULIS in PM2.5
868   emitted from biomass burning in traditional "Heated Kang" in Northwest China. Sci. Total
869   Environ. 776, 146014.

870 Zhang, T., Shen, Z., Zhang, L., Tang, Z., Zhang, Q., Chen, Q., Lei, Y., Zeng, Y., Xu, H., Cao, J., 2020.
871   PM2.5 Humic-like substances over Xi'an, China: Optical properties, chemical functional
872   group, and source identification. Atmos. Res. 234, 104784.

873 Zhang, W., Li, L., Wang, D., Wang, R., Yu, S., Gao, N., 2022c. Characterizing dissolved organic
874   matter in aquatic environments by size exclusion chromatography coupled with multiple
875   detectors. Anal. Chim. Acta 1191, 339358.

876 Zheng, G.J., He, K.B., Duan, F.K., Cheng, Y., Ma, Y.L., 2013. Measurement of humic-like substances
877   in aerosols: A review. Environmental Pollution 181, 301-314.

878 Zou, C., Cao, T., Li, M., Song, J., Jiang, B., Jia, W., Li, J., Ding, X., Yu, Z., Zhang, G., Peng, P.a., 2023.
879   Measurement report: Changes in light absorption and molecular composition of
880   water-soluble humic-like substances during a winter haze bloom-decay process in
881   Guangzhou, China. Atmos. Chem. Phys. 23, 963-979.

882 Zou, C., Li, M., Cao, T., Zhu, M., Fan, X., Peng, S., Song, J., Jiang, B., Jia, W., Yu, C., Song, H., Yu, Z.,
883   Li, J., Zhang, G., Peng, P.a., 2020. Comparison of solid phase extraction methods for the
884   measurement of humic-like substances (HULIS) in atmospheric particles. Atmos. Environ.
885   225, 117370.

886

887